AIAA 81-1269R

Turbulence Closure and Prediction of the Wake in a Rotating Wall Shear Layer

C. Hah*
The Pennsylvania State University, University Park, Pennsylvania

The turbulent wake interacting with the rotating wall shear layer is studied analytically and numerically. The pressure-strain correlation term in the Reynolds stress transport equation is remodeled to represent the effect of rotation. The standard correction for the near-wall effect is also incorporated in the modified Reynolds stress closure model. The rotation-modified Reynolds stress closure model is applied to predict the fully developed and the developing flows in a rotating duct and the three-dimensional wake developing in a rotating wall shear layer. The complex turbulent flow affected by the rotation and the wall damping is predicted with an accuracy sufficient for practical purposes.

Nomenclature

A	= constant in the law of the wall, Eq. (21)
C	= chord length of blade
$C_1, C_s, C_{\phi 1}, C_\epsilon,$ $C_{\epsilon 1}, C_{\epsilon 2}, \gamma, C_c$	= constants in turbulence closure models
E	= constant in the law of the wall, Eq. (21)
g_{ij}, g^{ij}	= metric tensor, Eq. (2)
k	= turbulence kinetic energy
P	= $\overline{u_i u_j} U^i_{,j}$
p	= static pressure
p'	= fluctuating component of static pressure
p^*	= reduced static pressure $[p-(\rho/2)r^2\Omega^2]$
R_i	= Richardson number for the curved turbulent flow
S	= blade spacing
S_l	= source term in the energy dissipation equation
s,n,r	= curvilinear coordinates (streamwise, normal, and radial direction, Fig. 1; $s=0$, $n=0$ is at the trailing edge of blade)
U,V,W	= streamwise, normal, and spanwise mean velocities (Fig. 1)
u,v,w	= fluctuating velocities in streamwise, normal, and spanwise velocities (Fig. 1)
U^i, u^i	= contravariant mean and fluctuating velocity component [U,V,W,u,v,w in (s,n,r) coordinates]
u^*	= friction velocity
$\overline{u^i u^i}$	= turbulence intensity with components $\overline{u^2}$, $\overline{v^2}$, $\overline{w^2}$ in s,n,r directions
$\overline{u^i u^j}$	= shear stress with components $\overline{uv}$, $\overline{uw}$, and $\overline{vw}$ in (s,n,r) coordinates
Ω	= angular speed of rotor
Ω_i	= angular velocity of rotor [$\Omega_s, \Omega_n, \Omega_r$ in (s,n,r) coordinates]
β	= angle between machine axis and streamwise direction (Fig. 1)
δ_{ij}	= Kronecker delta
ϵ	= turbulence energy dissipation rate
$\epsilon_{ijk}, \epsilon^{ijk}$	= permutation tensor
ν	= kinetic viscosity
ρ	= density
Γ^i_{jk}	= Christoffel symbol of second kind

Subscripts

c	= values at wake center
s,n,r	= streamwise, normal, and radial components, respectively (Fig. 1)
t	= values at blade tip
w	= values at the solid wall
0	= passage-averaged value
∞	= values in freestream

Superscripts

$(\bar{\ })$	= average value
$(\ )'$	= fluctuating quantity

Presented as Paper 81-1269 at the AIAA 14th Fluid and Plasma Dynamics Conference, Palo Alto, Calif., June 23-25, 1981; submitted July 20, 1981; revision received Jan. 15, 1982.

*Research Associate, Department of Aerospace Engineering; presently, Engineer, General Electric Corporate Research and Development Center, Schenectady, N. Y. Member AIAA.

Introduction

THE characteristics of the wake interacting with the wall shear layer are different from those of the free wake. Many experimental studies have shown that the defect of the wake decays more slowly for the wake interacting with the wall shear layer than it does for the free wake. Also, the turbulence characteristics are substantially altered by the effects of the rotation and the solid wall. These features of the flow cannot be successfully predicted with the turbulence closure schemes developed for the nonrotating free shear flow.

The three-dimensional turbulent wake developing very near the hub wall in a compressor is one of the most complex flowfields. The flow is affected by the rotation, streamline curvature, and the interaction between the wake and the wall shear layer. In the free wake, the flow diffusion occurs mainly across the wake, while the main diffusion occurs in the radial direction in the hub-wall boundary layer. Therefore, both the radial diffusion and the normal diffusion should be included in the governing equation for any reasonable prediction scheme. The importance of the flow near the hub wall or the annulus wall in the turbomachinery has been long recognized[1,2] and several prediction methods have been proposed.[1-3] However, these methods have been based on either inviscid secondary flow theory or conventional boundary-layer theory. Hence, accurate estimations of the friction, compressor performance, efficiency, etc., have not been expected. With the recent advancement of the numerical technique and the availability of a large computer, the numerical prediction of the whole flowfield inside a compressor has been planned based on the Navier-Stokes equation. The precise understanding of the flow characteristics through experimental study and proper turbulence closure modeling for the turbulent flow near the hub wall or annulus wall is essential for the overall flow prediction scheme.

Although the effect of rotation was recognized long ago (e.g., Taylor[4]), little work has been published to date. Johnston et al.[5] studied the effect of rotation on the turbulent boundary layer in the idealized passage of a centrifugal pump and found substantial change in the mean velocity profile as well as in the turbulence structure. They also gave a simple analysis of the effect of rotation based on their experiment. The effect of the rotation on the turbulent flowfield can be estimated approximately with the Rossby number (the ratio of Coriolis forces to inertia forces). The effect of rotation on the boundary layer of the axial compressor blade has been considered to be smaller than that of the centrifugal blade because the boundary layer of the axial compressor is thinner than that of the centrifugal compressor. However, the viscous layer in the interacting flow region is much thicker than the blade boundary layer, and the corresponding Rossby number is comparable with that of the centrifugal compressor boundary layer.

Few numerical studies for the rotating turbulent shear flow have been reported. Majumdar et al.[6] used the two-equation turbulence closure model for the prediction of the flow in a rotating duct. Their numerical study indicated that they could not properly predict the rotating turbulent flow without including the effect of rotation in the turbulence closure models. Howard et al.[7] modified the two-equation model for the effect of rotation. In their simple modification, the rate of turbulence energy dissipation is altered empirically to include the stabilizing and destabilizing effects of rotation. In the two-equation model, the rate of turbulence kinetic energy dissipation is handled as a scalar quantity rather than as a vector, and the change of this scalar quantity for the effect of rotation is physically conflicting. Also, when the flowfield is affected by the multicomponents of the Coriolis force, the selection of a nondimensional parameter for the rotation effect is difficult even for empirical purposes.

Near the wall, the level of fluctuating velocity normal to the surface is restrained, while the fluctuating component parallel to the wall is enhanced relative to the free shear flow. In the Reynolds stress closure model, this effect can be satisfactorily included in the turbulence closure model by modifying the pressure-strain correlation.[9-11] The turbulent wake of the rotor blade is like a jet when the flow is watched from an absolute frame and the present flow is an unsteady, three-dimensional turbulent wall jet when observed from an absolute frame. The slower rate of the wake defect decay is due to the solid wall effect or the restraint of the normal turbulence intensity. The wall effect correction of the pressure-strain term is incorporated in the presently used turbulence closure model, and the numerical results are compared with the experimental data.

The objective of the present study is to examine the characteristics of the rotor wake interacting with the hub-wall boundary layer using the experimental data and to modify the Reynolds stress closure for the effects of rotation and solid wall. The pressure-strain correlation is properly modeled for the effect of rotation. The modified Reynolds stress closure is used to predict the flow numerically, and a comparison between experimental data and predictions is made for the effect of rotation and solid wall on the complex turbulent flowfield.

Governing Equations and Coordinate System

The continuity and momentum equations governing the steady, incompressible, fully turbulent flow relative to a coordinate system rotating with angular velocity Ω_i are, in generalized tensor form,

$$U^i_{,i}=0, \qquad u^i_{,i}=0 \tag{1}$$

$$U^j U^i_{,j}+\overline{u^j u^i}_{,j}+2\epsilon^{ijk}\Omega_j U_k=-\frac{g^{ij}}{\rho}\frac{\partial p^*}{\partial x^j}+\nu g_{jk}U^i_{,jk} \tag{2}$$

where U^i and u^i are mean and fluctuating contravariant velocity components, respectively.

A turbulence closure model is required to describe the turbulence stress tensor $\overline{u^i u^j}$ appearing in the momentum equation. For the present study, a Reynolds stress closure model is applied and modified for the effects of rotation and solid wall. The exact transport equation of the Reynolds stress tensor is

$$U_k\overline{u^i u^j}_{,k}+\overline{u^j u_k}U^i_{,k}+\overline{u^i u_k}U^j_{,k}+\overline{u^i u^j}u_{k,k}+2\Omega_\ell\epsilon^{i\ell m}\overline{u_m u^j}+2\Omega_\ell\epsilon^{j\ell m}\overline{u_m u^i}=-\frac{1}{\rho}(\overline{u^j p'_{,j}}+\overline{u^i p'_{,j}})+\nu g_{ik}(\overline{u^j u^i_{,k}}+\overline{u^i u^j_{,k}}) \tag{3}$$

As this equation introduces further unknown turbulence correlations, these correlations are properly modeled for the closure of governing equations. As a second-order closure model, the turbulence correlations in the diffusion, pressure-strain, and dissipation terms are modeled with the Reynolds stress tensor, the mean shear rate, and the scalar dissipation rate (the divergence of the dissipation tensor). The pressure-strain correlation has three contributions for nonrotating flows, the first arising due to the mutual interaction of fluctuating velocities ($\phi_{ij,1}$), the second due to the interaction of the mean shear rate and fluctuating velocities ($\phi_{ij,2}$), and the third due to the solid wall effect (S_{ij}). For free shear flow, the third effect can be neglected. Rotta[12] proposed the following model for the first part:

$$(\phi_{ij}+\phi_{ji})_1=-c_1(\epsilon/k)(\overline{u_i u_j}-\tfrac{2}{3}\delta_{ij}k) \tag{4}$$

Naot, Savit, and Wolfshtein[13] and Launder, Reece, and Rodi[9] introduced the following model for the second part of pressure-strain correlation:

$$(\phi_{ij}+\phi_{ji})_2=\gamma(P_{ij}-\tfrac{2}{3}P\delta_{ij}) \tag{5}$$

where P_{ij} is the production of Reynolds stress $\overline{u_i u_j}$ and P the production of turbulence kinetic energy. A scalar dissipation rate is introduced for the modeling of the dissipation term with the assumption that the dissipation is due to isotropic small-scale turbulent motion at high Reynolds number.

Hanjalic and Launder[14] proposed a model for the diffusion term in Eq. (3). The full Reynolds stress model solves seven additional equations for the six nonzero Reynolds stress components and the dissipation rate. However, the application of this model to a three-dimensional flowfield is very expensive and complex and causes numerical instability for certain types of flow. Hah and Lakshminarayana[8] simplified the full Reynolds stress model by handling the convective and diffusion terms collectively, and introduced a variable to represent the collective effect of these two terms with the assumption that the collective effect is related to the production term. Then the simplified Reynolds stress model for free shear flow is

$$0=(1+C_1)(-\overline{u_k u^j}U^i_{,k}-\overline{u_k u^i}U^j_{,k})(1-\gamma)-2(\epsilon^{i\ell m}\Omega_\ell\overline{u_m u^j}+\epsilon^{j\ell m}\Omega_\ell\overline{u_m u^i})-\tfrac{2}{3}g^{ij}\epsilon(1-\gamma)-C_{\phi 1}(\epsilon/k)(\overline{u^i u^j}-\tfrac{2}{3}g^{ij}k) \tag{6}$$

where C_1 relates the collective effects of the convection and diffusion terms to the production term. The modeled Reynolds stress equation (6) includes a redistribution term due to the coordinate rotation, and the pressure-strain correlation is not properly modeled for the effect of rotation. The modification of the pressure-strain correlation for the effect of rotation and solid wall will be described in the following section.

With this model, the individual Reynolds stress components can be evaluated if the mean shear rate, turbulence kinetic

energy, and energy dissipation rate are known. The following partial differential equations are solved for the turbulence kinetic energy and energy dissipation rate:

$$U^i \frac{\partial k}{\partial x^i} = \frac{\partial}{\partial x^i}\left(\frac{\nu_{\text{eff}}}{\sigma_k}\frac{\partial k}{\partial x^i}\right) + P - \epsilon \tag{7}$$

$$U^i \frac{\partial \epsilon}{\partial x^i} = \frac{\partial}{\partial x^i}\left(\frac{\nu_{\text{eff}}}{\sigma_\epsilon}\frac{\partial \epsilon}{\partial x^i}\right) + S_l - C_{\epsilon 2}\frac{\epsilon^2}{k} \tag{8}$$

where

$$\nu_{\text{eff}} = C_\mu k^2/\epsilon, \qquad P = -\overline{u_i u_j} U^i_{,j}, \qquad k = \tfrac{1}{2} g_{ij}\overline{u^i u^j}$$

$$-\overline{u^i u^j} = \nu_{\text{eff}}\left(U^i_{,j} + U^j_{,i}\right) - \tfrac{2}{3} k g^{ij}$$

and S_l is the source term in the transport equation of the rate of turbulent kinetic energy dissipation. Hah and Lakshminarayana[15] introduced the following form of S_l to predict the curved turbulent flow correctly

$$S_l = C_\ell \frac{\epsilon^2}{k^3}\left(\overline{u^i u^j} - \tfrac{2}{3} k\delta_{ij}\right)\left(\overline{u^j u^i} - \tfrac{2}{3} k\delta_{ji}\right) \tag{9}$$

To predict the flowfield numerically, the governing continuity and momentum equations [(1) and (2)] along with the turbulence closure equations (6-8) should be solved on a convenient coordinate system. The development of the rotor wake near the hub wall is briefly explained in Fig. 1. The radial velocity, which is generated as a result of the imbalance of acting radial forces near the wake center, is restrained due to the hub wall. Near the hub wall, high normal velocity is observed due to the secondary flow effect. Away from the wall, the flow shows typical characteristics of a rotor wake and the approximate streamwise direction is easily defined on the cylindrical surface. A curvilinear coordinate for general flow near the hub wall is also shown in Fig. 1. S is the approximate streamwise direction on a cylindrical surface away from the wall, n the normal direction to the streamwise direction on a cylindrical surface, and r the radial direction. The derivation of this coordinate system and its application to the free rotor wake are given in Ref. 8. Although the present coordinate system is nonorthogonal, the boundary condition at the hub wall can be easily described with the present coordinates. Also, the governing equations can be simplified because the main flow direction is closely represented with one coordinate line.

Modification of Reynolds Stress Closure for the Effects of Rotation and Solid Wall

The effect of rotation has been qualitatively explained with the balance of the pressure gradient and the local mean Coriolis force. Based on a simple shear layer in a plane that rotates about an axis perpendicular to the plane of the flow, the argument is as follows. If a particle perturbed to an adjacent layer is forced to return to its original layer by the resultant force of the pressure gradient and the Coriolis force, the effect of rotation is to stabilize the flowfield and diminish the turbulent transportation. When the perturbed particle is accelerated away by the resultant force, the flow is destabilized. Bradshaw[16] derived the following gradient Richardson number as a local stability parameter:

$$R_i = \frac{-2\Omega[(\mathrm{d}U/\mathrm{d}y) - 2\Omega]}{(\mathrm{d}U/\mathrm{d}y)^2} \tag{10}$$

The above stability parameter does not include the viscosity effect, which may be substantial near the wall. The gradient

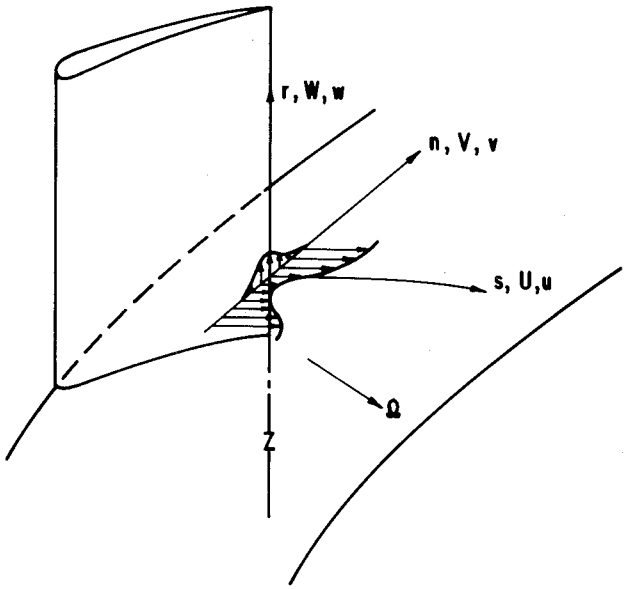

Fig. 1 Coordinate system and flow configuration.

Richardson number indicates the overall trend and cannot be used as a quantitative measure of the rotation effect. Howard et al.[7] used the above nondimensional parameter to modify the dissipation equation of the k-ϵ model to determine the effect of rotation empirically. As the Richardson number does not represent the quantitative effect of rotation, the universal constant tuned for a specific rotating flow may not be applicable to a wide range of flows. Furthermore, the selection of the proper nondimensional parameter is very difficult when the flow is three-dimensional and the multiple component of the Coriolis force is involved.

The modeled Reynolds stress transport equation (6) includes a redistribution term due to the coordinate rotation. This model was used by Hah and Lakshminarayana[8] to predict the free rotor wake. Although the prediction was satisfactory, the effect of rotation was not sufficiently represented with this model. Among the various terms in Eq. (3), the pressure-strain correlation term is directly affected by the rotation, and this term should be properly modeled to include the effect of rotation in the turbulence closure.

The explicit appearance of the pressure in the pressure-strain correlation can be eliminated by taking the divergence of the equation for the fluctuating velocity u_i. The resulting Poisson equation for the rotating flow is in Cartesian tensor

$$\frac{1}{\rho}\frac{\partial^2 P}{\partial x_i \partial x_i} = -2U_{i,j}u_{j,i} + \left(\overline{u_i u_j} - u_i u_j\right)_{,ij} - 2\epsilon_{ijk}\Omega_j u_{k,i} \tag{11}$$

Using the general solution of the above Poisson equation, the pressure-strain correlation for rotating flow is

$$\overline{\frac{p}{\rho}\frac{\partial u_i}{\partial x_j}} = \frac{1}{4\pi}\int_{\text{vol}} \Bigg[\underbrace{\left(\overline{\frac{\partial^2 u_l u_m}{\partial x_l \partial x_m}}\right)'\frac{\partial u_i}{\partial x_j}}_{\phi_{ij,1}} + \underbrace{2\left(\frac{\partial U_l}{\partial x_m}\right)'\left(\overline{\frac{\partial u_m}{\partial x_l}}\right)'\left(\overline{\frac{\partial u_i}{\partial x_j}}\right)}_{\phi_{ij,2}}\Bigg]\frac{\mathrm{d\,vol}}{|x-y|}$$

$$+ \underbrace{\frac{1}{4\pi}\int_{\text{vol}} 2(\epsilon_{\ell nm}\Omega_n)\left(\overline{\frac{\partial u_\ell}{\partial x_m}}\right)'\left(\overline{\frac{\partial u_i}{\partial x_j}}\right)\frac{\mathrm{d\,vol}}{|X-Y|}}_{\phi_{ij,3}} + S_{ij} \tag{12}$$

where terms with and without a prime relate to values at Y and X, respectively (the integration being carried out over Y space), and S_{ij} is a surface integral.

The modeling of $\phi_{ij,1}$ and $\phi_{ij,2}$ in Eq. (12) was already introduced as Eqs. (4) and (5). The modeling of $\phi_{ij,3}$, which is due to the rotation, is obtained using an approximation similar to the one used for the simulation of $\phi_{ij,2}$. Following Rotta's work,[12] $\phi_{ij,3}$ is approximated as

$$\phi_{ij,3} = \Omega_n \epsilon_{\ell nm} a_{\ell j}^{mi} \tag{13}$$

where

$$a_{\ell j}^{mi} = -\frac{1}{2\pi} \int_{\text{vol}} \frac{\partial^2 \overline{u_m' u_i}}{\partial r_\ell \partial r_j} \frac{\text{d vol}}{dr}$$

and

$$r = Y - X; \qquad r = |r|$$

Various assumptions for $a_{\ell j}^{mi}$ used in the simulation of $\phi_{ij,2}$ can be used again for the modeling of $\phi_{ij,3}$. Launder, Reece, and Rodi[9] derived the following of the fourth-order tensor $a_{\ell j}^{mi}$ based on the kinematic constraints,

$$a_{\ell j}^{mi} = D_1 \delta_{\ell j} \overline{u_m u_i} + D_2 (\delta_{m\ell} \overline{u_i u_j} + \delta_{mj} \overline{u_i u_\ell} + \delta_{i\ell} \overline{u_m u_j} + \delta_{ij} \overline{u_m u_\ell})$$
$$+ D_3 \delta_{mi} \overline{u_\ell u_j} + [D_4 \delta_{mi} \delta_{\ell j} + D_5 (\delta_{m\ell} \delta_{ij} + \delta_{mj} \delta_{i\ell})] k \tag{14}$$

where the constants D_1, D_2, D_4, and D_5 are expressed in terms of D_3,

$$D_1 = \frac{1}{11}(4D_3 + 10), \qquad D_2 = -\frac{1}{11}(2 + 3D_3)$$

$$D_4 = -\frac{1}{55}(50D_3 + 4), \qquad D_5 = \frac{1}{55}(20D_3 + 6) \tag{15}$$

Then, from Eqs. (13) and (14),

$$\phi_{ij,3} = D_1 \Omega_n \epsilon^{jnm} \overline{u_m u_i} + D_2 \Omega_n (\epsilon^{\ell nj} \overline{u_i u_\ell} + \epsilon^{inm} \overline{u_m u_j}$$
$$+ \epsilon^{\ell nm} \delta_{ij} \overline{u_m u_\ell}) + D_3 \Omega_n \epsilon^{\ell ni} \overline{u_\ell u_j} + (D_4 \Omega_n \epsilon^{jni} + D_5 \Omega_n \epsilon^{inj}) \tag{16}$$

Therefore, the complete influence of the rotation on the pressure-strain correlation can be expressed in a generalized tensor as

$$(\phi_{ij} + \phi_{ji})_3 = D_6 \Omega_n (\epsilon^{\ell ni} \overline{u_\ell u^j} + \epsilon^{\ell nj} \overline{u_\ell u^i}) \tag{17}$$

where

$$D_6 = \frac{7}{11} D_3 - \frac{10}{11}$$

The experimental data by Johnston, Halleen, and Lezins[5] on a simple rotating shear flow are used to evaluate the constant D_6 (or D_3). The modeled Reynolds stress equation (6), combined with Eq. (17) for the rotation effect, can be written for nonzero stress components as

$$-\overline{uv} = (1 + C_1) k (1 - \gamma) \left(\overline{v^2} \frac{\partial U}{\partial y} \right) \Big/ (C_{\phi 1} \epsilon)$$
$$+ (2 - D_6) \Omega (\overline{u^2} - \overline{v^2}) k / (C_{\phi 1} \epsilon) + [\text{O.T.}] \tag{18a}$$

$$\overline{u^2} = (1 + C_1) k (1 - \gamma) \left(-2\overline{uv} \frac{\partial U}{\partial y} \right) \Big/ (C_{\phi 1} \epsilon)$$
$$- 2(2 - D_6) k \Omega (-\overline{uv}) / (C_{\phi 1} \epsilon) + [\text{O.T.}] \tag{18b}$$

$$\overline{v^2} = 2(2 - D_6) k \Omega (-\overline{uv}) / (C_{\phi 1} \epsilon)$$
$$- \tfrac{2}{3} k (1 - \gamma + C_{\phi 1}) / C_{\phi 1} + [\text{O.T.}] \tag{18c}$$

$$\overline{w^2} = \tfrac{2}{3} k (1 - \gamma) / C_{\phi 1} + \tfrac{2}{3} C_{\phi 1} k + [\text{O.T.}] \tag{18d}$$

where [O.T.] represents smaller terms not presented in Eqs. (18). Various values of D_6 were tried along with Eqs. (7) and (8), and the optimum value of D_6 was 0.7 for the experimental data used.

Figure 2 shows the comparison between experimental data and prediction with the present model for the turbulent eddy viscosity. The distribution of the turbulent eddy viscosity is well predicted for both the rotating and nonrotating flows. Similar results have been obtained by modifying the transport equation of the turbulence energy dissipation.[7] However, the present model can be used for general three-dimensional flow, where multiple components of the Coriolis force are involved.

Near the solid wall, the turbulence structure is altered by the so-called damping effect of the wall. The fluctuating velocity is restrained, while that parallel to the main flow is enhanced compared to the free shear flow. Near the wall, convection and diffusion terms are negligibly small compared to the other terms. Then the relative magnitude of the normal stresses are approximately decided by the pressure-strain correlation. Therefore, the pressure-strain correlation should be properly modeled for the solid wall effect. Various proposals have been made for the wall correction in the pressure-strain correlation. For the present study, the additive terms utilized for wall correction previously used by Gibson and Launder[11] are

$$(\phi_{ij} + \phi_{ji})_{,w} = C_1' (\epsilon/k) \left(\overline{u_n^2} \delta_{ij} - \frac{3}{2} \overline{u_n u_i} \delta_{nj} \right.$$
$$\left. - \frac{3}{2} \overline{u_n u_j} \delta_{ni} \right) (k^{3/2} / C_w Y \epsilon) + \gamma' \left(\phi_{nn,2} \delta_{ij} - \frac{3}{2} \phi_{ni,2} \delta_{nj} \right.$$
$$\left. - \frac{3}{2} \phi_{nj,2} \delta_{ni} \right) (k^{3/2} / C_w Y \epsilon) \tag{19}$$

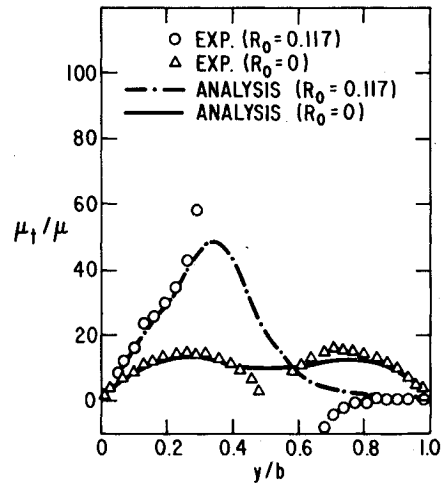

Fig. 2 Comparison of predicted turbulent eddy viscosity with experimental data (measurement by Johnston et al.[5]).

Table 1 Constants in the turbulence closure model

$C_s = 0.1$	$\gamma = 0.6$
$C_1 = 1.5$	$D_6 = -0.7$
$C_\epsilon = 0.15$	$C_1' = 0.75$
$C_{\epsilon 1} = 1.45$	$\gamma' = 0.45$
$C_{\epsilon 2} = 1.9$	$C_w = 4.4$

In these expressions, n represents the direction normal to the wall and y is the distance from the wall.

The final modeled Reynolds-stress equation is obtained by combining Eqs. (6), (17), and (19) as follows:

$$0 = (1+C_1)(-\overline{u_k u^j} U^i_{,k} - \overline{u_k u^i} U^j_{,k})(1-\gamma) - 2(\epsilon^{i\ell m}\Omega_\ell \overline{u_m u^j} + \epsilon^{j\ell m}\Omega_\ell \overline{u_m u^i}) - \tfrac{2}{3} g^{ij}(1-\gamma) - C_{\phi 1}\frac{\epsilon}{k}(\overline{u^i u^j} - \tfrac{2}{3} g^{ij} k) + D_6 \Omega_n (\epsilon^{\ell n i}\overline{u_\ell u^j} + \epsilon^{\ell n j}\overline{u_\ell u^i}) + (\phi_{ij} + \phi_{ji})_{,w} \quad (20)$$

Various constants in the turbulence closure equations have not been optimized for the present study, except for D_6 in Eq. (17). All the constants are compiled in Table 1.

Numerical Scheme and Boundary Conditions

The rotating wake interacting with the wall shear layer was predicted mainly to verify the turbulence closure model for the effects of rotation and solid wall. Near the junction of the trailing edge of the blade and the hub wall, the flow is very complex due to the large amount of secondary flow and possibly the corner vortex, and usually contains a separated flow region. Recent experimental study of this flow by Hah and Lakshminarayana[17] with the multisensor hot-wire probe showed the highly complicated nature of the flow. The experimental data very near the trailing edge may not have been fully utilized for verification purposes.

For the present study, the calculation domain started at 30% chord downstream of the blade trailing edge and maximum streamwise mean velocity defect was 40% of the freestream velocity. Therefore, a severe streamwise velocity gradient or any recirculating region was not involved for the present computation domain. The streamwise diffusion, which is relatively small compared to the normal and radial diffusion in the present computation domain, was neglected, and the governing equations were solved downstreamwise in a parabolized scheme. The computation domain is shown in Fig. 3. The distance AB was 15% of the passage height between the hub and annulus walls. The outlet surface EFGH was 1.6 chord distance downstream of the blade trailing edge. With the utilized numerical scheme, boundary conditions were required on the surfaces ABCD, BCGF, ABFE, CDHG, and ADHE. Due to the nature of the flow in a compressor, a periodic boundary condition was applied between the planes ABFE and CDHG; that is, the distribution of flow quantities on the surface ABFE was the same as that on the surface CDHG. The boundary conditions on the surfaces ABCD and BCGF were based on the experimental data and the correlations of the experimental data. The solid wall boundary condition was applied on the surface ADHE.

The present turbulence closure model is valid only at high Reynolds number, even though wall correction is utilized. Further, the turbulence correlations are not properly described with the present model very near the solid wall. To utilize the present turbulence closure model for the entire flow region, a wall function was introduced near the solid wall.[18] The finite-difference nodes nearest to the solid wall were located in the inertial sublayer, where the production and dissipation of the turbulence kinetic energy is balanced and the law of the wall is valid. Then the relations obtained for the

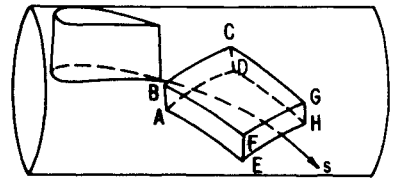

Fig. 3 Computation domain.

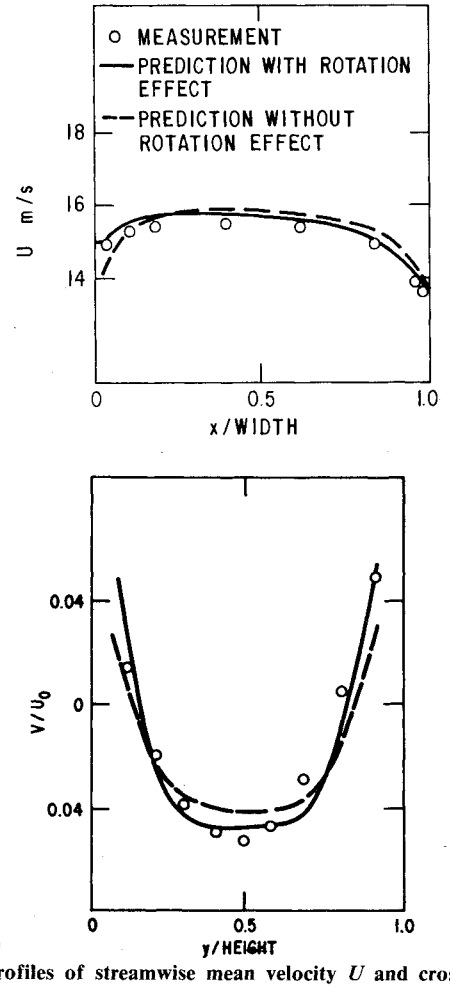

Fig. 4 Profiles of streamwise mean velocity U and cross-passage mean velocity V at passage centerline (measurement by Wagner and Velkoff[19]).

boundary condition at these points are

$$\frac{U}{u_*} = \frac{1}{A}\ell n\left(\frac{u_* y}{\nu}E\right), \qquad A = \frac{u_*^2}{\sqrt{C_u}}, \qquad \epsilon = \frac{u_*^3}{A/y} \quad (21)$$

where u is the friction velocity, ν the kinematic viscosity, and A and E constants. As the streamwise pressure gradient in the present calculation domain was moderate, no pressure correction was used in the law-of-the-wall equation.

Comparison between the Numerical Predictions and the Experimental Data

The present turbulence closure model was first used to predict the developing flow in a rotating rectangular duct. The experimental data by Wagner and Velkoff[19] of the turbulent flow in a low-aspect-ratio duct was used for the comparison purpose because the flow is affected by the secondary flow and pressure gradient in addition to the rotation effect. The duct was 0.864 m in length with a nozzle at the duct exit. The rectangular cross section had a height of 0.0445 m and a width

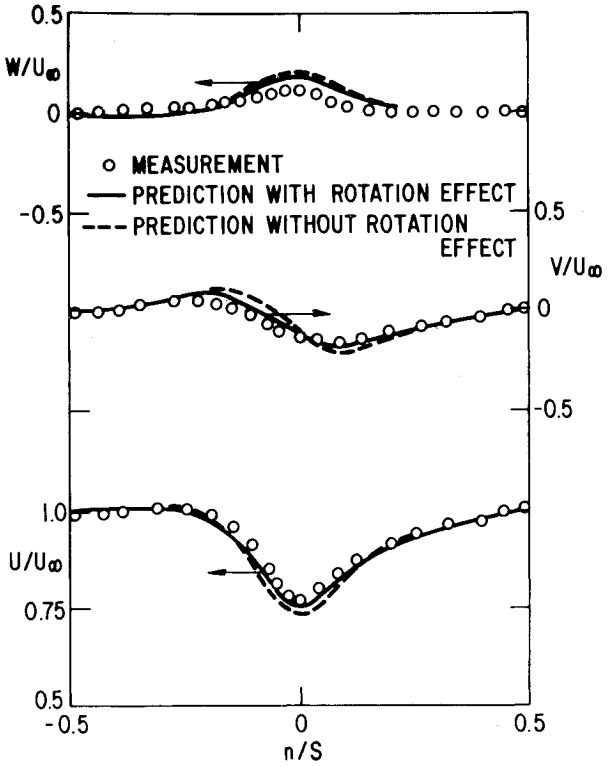

Fig. 5 Profiles of mean velocity components at $r/r_t = 0.512$ and $s/C = 0.87$ (measurement by Hah and Lakshminarayana[17]).

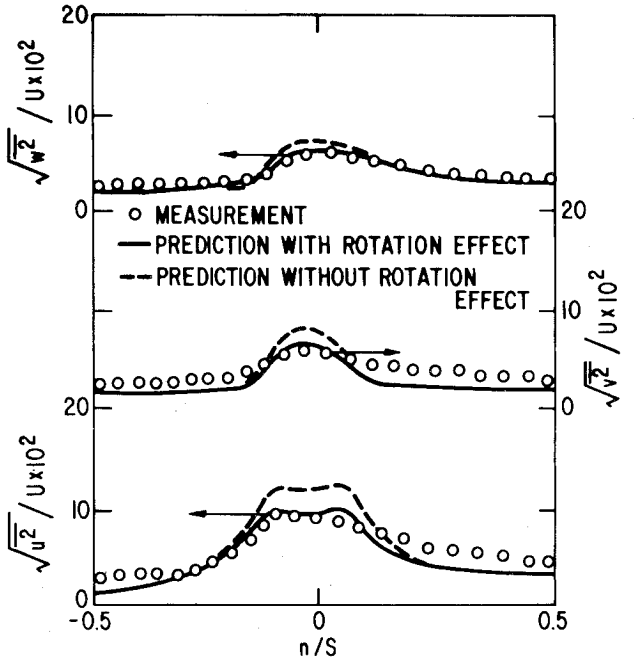

Fig. 6 Profiles of turbulence intensity at $r/r_t = 0.512$ and $s/C = 0.87$ (measurement by Hah and Lakshminarayana[17]).

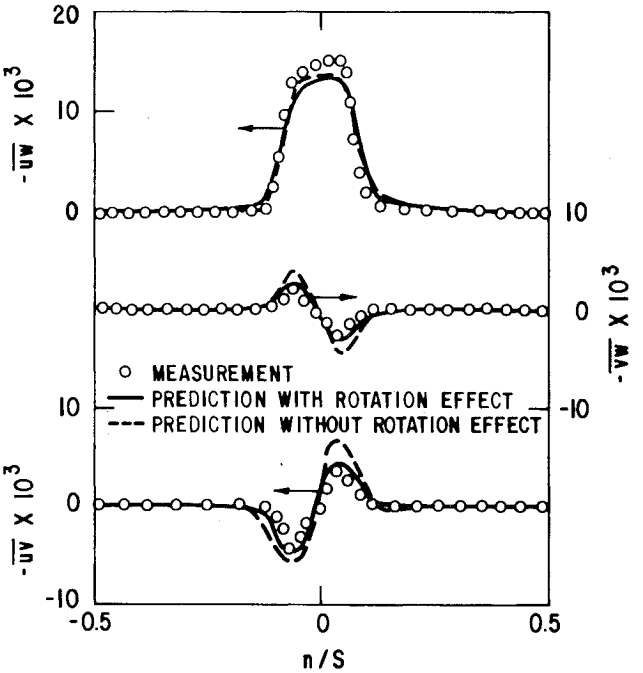

Fig. 7 Profiles of turbulent shear stress at $r/r_t = 0.512$ and $s/C = 0.87$ (measurement by Hah and Lakshminarayana[17]).

of 0.121 m. The computation started from the duct entrance with the assumption of the uniform velocity distribution. The computation employed a 20×22 grid at cross section and 28 steps were used downstream. The comparison of mean velocity profile between experimental data and numerical prediction was made at 0.61 m from the entrance and is shown in Fig. 4. Figure 4a shows the comparison of streamwise velocity profile at the midheight of the passage at the rotational speed of 300 rpm. The numerical prediction shows clearly the difference of velocity profiles between the pressure side and the suction side of the duct. When the effect of the rotation is not included in the turbulence modeling, more symmetric distribution of streamwise velocity is predicted because the turbulence eddy viscosity is not affected by the rotation. The cross-passage velocity profile on the passage centerline is compared in Fig. 4b. The comparison in Fig. 4 indicates that the effect of rotation on the developing turbulent flow in a low-aspect-ratio duct is very well represented through the present turbulence closure scheme, although the flow is very complex due to the high secondary flow and pressure gradient.

The experimental data of the rotor wake developing near the hub wall[17] in a single-stage compressor was used to verify the present turbulence closure model for the effects of the rotation and the near wall. Some relevant data of the compressor are: hub/tip ratio = 0.5, number of blades = 21, blade code/spacing at midradius = 1.35, tip radius = 0.46 m, and stagger angle at midradius = 30 deg. The compressor was operated at 1066 rpm and the incidence angle at midradius was 7 deg. Various curve-fitting functions were used to describe the distribution of mean velocity and turbulence kinetic energy on the inlet surface. The mean velocity components were described with the Gauss distribution and a fourth-order polynomial. The linear distribution of the turbulence kinetic energy in the radial direction was assumed near the wall. The production and the dissipation of the turbulence kinetic energy was assumed to be balanced at the inlet surface. The comparison between the experimental data and the numerical prediction was made at $s/C = 0.87$ and 0.0025 m from the wall ($r/r_t = 0.512$). At this location, the measured angle between the machine axis and the streamline at the wake center was 8 deg at $r/r_t = 0.512$ and 28 deg at midradius. The velocity profiles are considerably skewed in the radial direction and the effect of rotation is not small. The comparison in mean velocity profile is given in Fig. 5. The mean velocity profiles are very well predicted when the effect of rotation is included in the turbulence closure modeling. When the effect of rotation is not included [the rotation related terms in Eq. (20) are omitted], considerable discrepancy in velocity profiles are observed in both the suction and the pressure sides of the wake. The experimental data show that the velocity defect in the wake center was

about 20% at this axial location, and the recovery rate of the mean velocity defect was slower than those of free wakes at the similar incidence angle. This slower decay rate is due to the solid wall effect, as properly predicted with the present numerical scheme. Even though some discrepancy is observed, especially near the wall, the overall development is well predicted. The comparisons in the Reynolds stress distribution at $s/C=0.87$ and 0.0025 m from the wall are given in Figs. 6 and 7. The overall trend of Reynolds stress distribution is not properly predicted when the effect of rotation is not included in the turbulence closure modeling.

The radial turbulence intensity ($\overline{w^2}$) is increased by the rotation away from the wall.[8] However, this component is damped by the solid wall effect. These trends are well observed in the experimental data and are properly predicted. The shear stress $-\overline{uv}$ is decreased when $-\overline{uw}$ is positive due to rotation, and the ratio of $-\overline{uv}/-\overline{uw}$ is consequently decreased by the rotation. This trend is also properly predicted with the present turbulence closure model.

Conclusions

A modified version of the Reynolds stress turbulence closure model was derived which accounts for the effects of rotation and wall damping. The pressure-strain correlation in the Reynolds stress transport equation was remodeled for the effect of rotation. The new model with the tensor-invariant representation of the rotation effect was shown to represent the effect of rotation accurately for the simple rotating shear flow. Also, the developing shear flow in a rotating duct was very well predicted with the present model. The three-dimensional rotating turbulent wake developing near the solid wall was also predicted with the developed turbulence closure model. The complex turbulent flow structure affected by the rotation and wall damping was predicted with an accuracy sufficient for practical purposes.

Acknowledgments

This work was supported by the National Aeronautics and Space Administration through Grant NSG 3266. Dr. P. Sockol was the technical monitor; his constructive comments are greatly appreciated. The author is also indebted to Prof. B. Lakshminarayana for his counsel and encouragement during the course of this investigation.

References

[1] Horlock, J. H., "Annulus Wall Boundary Layer in Axial Compressor Stages," *Transactions of ASME, Journal of Basic Engineering,* Vol. 85, 1963, pp. 55-65.

[2] Mellor, G. L. and Wood, G. M., "An Axial Compressor End Wall Boundary Layer Theory," *Transactions of ASME, Journal of Basic Engineering,* Vol. 93, 1971, pp. 300-316.

[3] Railly, J. W. and Sharma, P. B., "Treatment of Annulus Wall Boundary Layer Using a Secondary Flow Hypothesis," ASME Paper 76-GT-52, 1976.

[4] Taylor, G. I., "Stability of a Viscous Liquid Contained Between Two Rotating Cylinders," *Philosophical Transactions of the Royal Society of London,* Series A, Vol. 223, 1923, pp. 289-343.

[5] Johnston, J. P., Halleen, R. M., and Lezins, D. K., "Effects of Spanwise Rotation on the Structure of Two-Dimensional Fully Developed Turbulent Channel Flow," *Journal of Fluid Mechanics,* Vol. 56, Pt. 3, Dec. 1972, pp. 533-558.

[6] Majumdar, A. K., Pratrap, V. S., and Spalding, D. B., "Numerical Computation of Flows in Rotating Ducts," *Transactions of ASME, Journal of Fluids Engineering,* Vol. 99, March 1977, pp. 148-153.

[7] Howard, J. H. G., Patankar, S. V., and Vordunuik, R. M., "Flow Prediction in Rotating Ducts Using Coriolis-Modified Turbulence Models," *Transactions of ASME, Journal of Fluids Engineering,* Vol. 102, Dec. 1980, pp. 456-461.

[8] Hah, C. and Lakshminarayana, B., "Numerical Analysis of Turbulent Wakes of Axial Flow Turbomachinery Rotor Blades," Proceedings of the Symposium on "Turbulent Boundary Layers," *Transactions of ASME, Journal of Fluids Engineering,* Vol. 102, Dec. 1980, pp. 462-472.

[9] Launder, B. E., Reece, G. J., and Rodi, W., "Progress in the Development of a Reynolds Stress Turbulence Closure," *Journal of Fluid Mechanics,* Vol. 68, 1975, pp. 537-566.

[10] Daly, B. J. and Harlow, F. H., "Transport Equations of Turbulence," *Physics of Fluids,* Vol. 13, 1970, p. 2634.

[11] Gibson, M. M. and Launder, B. E., "Ground Effects on Pressure Fluctuations in the Atmospheric Boundary," *Journal of Fluid Mechanics,* Vol. 86, 1978, p. 491.

[12] Rotta, J. C., "Statische Thorie Nichthomogener Turbulenz," *Journal of Physics,* Vol. 129, 1976, p. 547.

[13] Naot, D., Shavit, A., and Wolfshtein, M., "Interactions Between Components of the Turbulent Velocity Correlation Tensor," *Israel Journal of Technology,* Vol. 8, 1970, p. 259.

[14] Hanjalic, K. and Launder, B. E., "A Reynolds-Stress Model of Turbulence and Its Application to Thin Shear Flows," *Journal of Fluid Mechanics,* Vol. 52, 1972, p. 609.

[15] Hah, C. and Lakshminarayana, B., "Prediction of Two- and Three-Dimensional Asymmetric Turbulent Wakes, Including Curvature and Rotation Effects," *AIAA Journal,* Vol. 18, Oct. 1980, pp. 1196-1204.

[16] Bradshaw, P., "The Analogy Between Streamline Curvature and Buoyancy in Turbulent Shear Flow," *Journal of Fluid Mechanics,* Vol. 36, Pt. 1, 1969, pp. 177-191.

[17] Hah, C. and Lakshminarayana, B., "Experimental and Numerical Study of the Viscous Flow Near the Hub Wall in a Rotor Passage," in preparation.

[18] Launder, B. E. and Spalding, D. B., "The Numerical Computation of Turbulent Flow," *Numerical Methods in Applied Mechanics and Engineering,* Vol. 3, 1974, p. 269.

[19] Wagner, R. E. and Velkoff, H. R., "Measurement of Secondary Flows in a Rotating Duct," *ASME Journal of Engineering for Power,* Vol. 94, Oct. 1972, pp. 261-270.